MITIGATION OF MOTION SICKNESS IN ROTORCRAFT BY USING H_∞-CONTROL

Süleyman Özkurt Research Associate
Sebastian Strobach Graduate Student
Tim Burkhardt Research Associate
Walter Fichter Professor

University of Stuttgart
Stuttgart, Germany

ABSTRACT

Motion sickness is a medical condition that presents with symptoms including nausea, disorientation, and vomiting. The condition is triggered by motion frequencies below 0.5 Hz, which affect the sensory organs of the passengers. The symptoms manifest over several minutes to hours and decrease when the motion exposure is terminated. In rotorcraft, low-amplitude, broadband rigid-body vibrations, caused by atmospheric disturbances, are the primary source of motion sickness. These vibrations are a reflexive response of the automatic flight control system and the pilot to atmospheric disturbances. A negative impression of the helicopter ride quality is likely to result if motion sickness is provoked during the flight. It is therefore beneficial to reduce the magnitude of the motions contributing to motion sickness. This can be achieved primarily through the disturbance rejection properties of the flight control system. Therefore, a systematic design procedure within the H_∞ control framework is applied to shape the disturbance rejection properties of the flight control system, thus reducing the severity of motion sickness while complying with relevant requirements such as stability and handling qualities. The simulation results indicate a good performance of the H_∞-controller in reducing motion sickness while achieving level 1 handling qualities. Consequently, the proposed systematic design procedure is a promising approach to improve the ride comfort in rotorcraft.

INTRODUCTION

In rotorcraft, two different phenomena can cause passenger discomfort. First, in the frequency range of 0.5 - 80 Hz, rotor-induced vibrations and tail-boom movements can result in whole-body vibrations (WBVs) of the passenger that reduce the perceived ride comfort. To reduce WBVs, rotorcraft engineers have developed active and passive countermeasures, which are described in Refs. 1–4. In general, WBVs are already well-managed in the rotorcraft industry. Motion sickness (MS), also known as kinetosis, is the second phenomenon that can cause passenger discomfort. Symptoms of MS can significantly diminish the flight experience. As stated by Griffin (Ref. 5, ch. 7), the severity of MS depends on the physical properties of the motion stimuli, individual characteristics, and the presence of visual information. According to Wada (Ref. 6), MS is provoked by low-frequency vibrations of 0.05 - 0.5 Hz that affect the sensory organs of the human body. In rotorcraft, MS is triggered due to the compensation reactions of the automatic flight control system (AFCS) and the pilot to atmospheric disturbances. As shown in Ref. 7, a bad choice of flight control parameters can increase the severity of MS. Unfortunately, current AFCS design procedures (Ref. 8) do not consider MS due to a lack of design requirements and the focus on meeting the stability and handling quality requirements from Refs. 9,10. However, handling qualities are becoming secondary to ride quality as rotorcraft automation increases. Consequently, the design of future AFCSs should be optimized regarding MS to enhance ride comfort.

The lack of design requirements for MS makes it difficult to optimize or design AFCSs in this respect. Therefore, this topic has to be approached heuristically. As stated by Griffin (Ref. 5, ch. 7), the severity of the MS symptoms increases linearly with the vibrational magnitudes. Hence, suppressing these vibrations over a wide range of frequencies is a key factor in reducing MS. The disturbance rejection properties of the AFCS, such as the disturbance rejection bandwidth (DRB) and the disturbance rejection peak (DRP), are crucial for the suppression of vibrations. The DRB and DRP are derived in Ref. 11 from the sensitivity functions of the hold variables and quantify the ability to suppress the disturbances. Consequently, it is stated that the severity of MS can be reduced by adequately shaping the sensitivity functions, i.e., the disturbance rejection properties of the AFCSs. A control method that allows the shaping of the sensitivity functions systematically is given by H_∞-control. Moreover, another benefit is the simple inclusion of the stability and handling quality requirements into the H_∞ optimization framework as shown in Ref. 4. Since most of these requirements can be expressed as specifications on the magnitude of the sensitivity and complementary sensitivity functions, the design space is constrained. These constraints can be met by appropriate definitions of weighting functions for the sensitivity and complementary sensitivity function within the H_∞ optimization framework. The mixed-sensitivity approach (i.e., shaping of sensitivity and complementary sensitivity function) allows the user to trade off robustness and system performance at the same time. This mixed-sensitivity approach of H_∞-control is used within this work to design an attitude command attitude hold (ACAH) controller for a rotorcraft. Controller synthesis is achieved through an iterative process of minimizing the H_∞-norm of the transfer function T_{zw}. This function describes the transfer behavior from the exogenous signals w to the error signals z. According to the algorithm in Ref. 12, linear matrix inequalities (LMIs) are used to minimize the H_∞ norm. The algorithm provides an internally stable controller that satisfies the condition $||T_{zw}||_\infty \leq \gamma$, where γ is a threshold that can be selected for the H_∞-norm. The reader is referred to Refs. 12–14 for a detailed description of the H_∞-control theory. In the context of the H_∞ framework, the $S/KS/T$ weighting scheme (Ref. 14) is the most prevalent approach. The $S/KS/T$ methodology shapes the sensitivity function S, the complementary sensitivity function T, and the product $K \cdot S$ to align with actuator specifications. As shown by Christen (Ref. 14, ch. 7), a disadvantage of the $S/KS/T$ weighting scheme is the inversion of the plant dynamics. This inversion leads to pole-zero cancellations of stable poles of the plant as stated in Refs. 14, 15. In rotorcraft, the aforementioned cancellations are problematic due to the presence of weakly damped modes, such as the phugoid and dutch-roll. Consequently, the GS/T weighting scheme from Refs. 4, 14 is used in this work to avoid the inversion of the plant dynamics. Within the GS/T weighting scheme, the product $G \cdot S$ is shaped, which makes existing weighting approaches unusable since they are only used to shape S. Findings in Ref. 4 suggest weighting approaches for the product $G \cdot S$. It is assumed that the appropriate shaping of the sensitivity function will result in a reduction of the severity of MS. The primary characteristics of the sensitivity function are bandwidth and peak value. As shown in Ref. 7, the arbitrary adjustment of the bandwidth is unlikely to lead to the mitigation of MS due to the waterbed effect. A systematic approach is necessary to reduce MS. As stated in Ref. 16, the severity of MS depends on the magnitudes of the translational accelerations and attitude angles. Since the focus lies on an ACAH controller, a systematic approach is derived by linking MS to the sensitivity functions of the attitude angles. Consequently, the primary contributions of this paper are:

- The derivation of the relationship between motion sickness and the sensitivity functions of the attitude angles.
- Systematic design procedure of an ACAH controller for rotorcraft incorporating motion sickness, stability and handling quality requirements.

The paper is structured as follows. First, the nominal helicopter model is introduced for the controller design. Second, the motion sickness model is presented. Third, the controller design objectives are described. Fourth, the results of the controller synthesis are illustrated. Then the simulated sickness results are presented for different controllers. Finally, conclusions are drawn from the results.

NOMINAL HELICOPTER MODEL

The nominal helicopter model is derived from the linearized equations of motion of a light four-bladed conventional helicopter, trimmed at 30 kt during level flight. The linearized equations of motion consist of nine rigid-body states and 18 rotor states. The rigid-body states are the translational velocities u, v, w, the angular velocities p, q, r, the attitude angles ϕ, θ, ψ. The rotor states contain the blade flapping, the blade lead-lag, and the blade torsion, which are represented in multi-blade coordinates. Under the assumption of a quasi-steady rotor, i.e., $\dot{x}_R = 0$, the state-space representation of the bare airframe is given as follows

$$\begin{aligned} \dot{x}_F &= A_{\text{red}} \cdot x_F + B_{\text{red}} \cdot u, \\ y &= C \cdot x_F, \end{aligned} \tag{1}$$

where A_{red} is 9×9 reduced state matrix, B_{red} is the 9×4 reduced input matrix, and C is 9×9 identity matrix. The state vector contains the rigid-body states $x_F = [u, v, w, p, q, r, \phi, \theta, \psi]^T$. The input vector u is represented by percentage values of the controls in the collective axis $d\theta$, the lateral axis $d\alpha$, the longitudinal axis $d\beta$, and the yaw axis $d\delta$. The authority of the helicopter control is restricted to ± 50 % To simplify the controller design and to meet relevant requirements from ADS33 (Ref. 9), axis decoupling is applied to the bare airframe model. Since the rotorcraft consists of four control channels, only four states can be decoupled. The decoupled states are chosen as $y_{\text{dec}} = [w, \phi, \theta, \psi]^T$ to comply with an ACAH controller. Consequently, the output equation is rewritten as

$$y_{\text{dec}} = \tilde{C} \cdot x_F = C_{\text{dec}} \cdot C \cdot x_F. \tag{2}$$

The approach from Ref. 17 is applied to decouple the inputs and states. The decoupling approach is based on differentiating the output Eq. (2) until the control inputs appear. Afterwards, the following state-space system is obtained

$$\begin{aligned} \dot{x}_F &= A_{\text{red}} \cdot x_F + B_{\text{red}} \cdot u, \\ y_D &= C_D \cdot x_F + D_D \cdot u. \end{aligned} \tag{3}$$

The vector y_D represents the derivatives of the states y_{dec}. The matrices C_D and D_D are defined as follows

$$C_D = \begin{bmatrix} \tilde{c}_1^T \cdot A_{\text{red}}^{\delta_w} \\ \tilde{c}_2^T \cdot A_{\text{red}}^{\delta_\phi} \\ \tilde{c}_3^T \cdot A_{\text{red}}^{\delta_\theta} \\ \tilde{c}_4^T \cdot A_{\text{red}}^{\delta_\psi} \end{bmatrix}, \; D_D = \begin{bmatrix} \tilde{c}_1^T \cdot A_{\text{red}}^{\delta_w - 1} \cdot B_{\text{red}} \\ \tilde{c}_2^T \cdot A_{\text{red}}^{\delta_\phi - 1} \cdot B_{\text{red}} \\ \tilde{c}_3^T \cdot A_{\text{red}}^{\delta_\theta - 1} \cdot B_{\text{red}} \\ \tilde{c}_4^T \cdot A_{\text{red}}^{\delta_{psi} - 1} \cdot B_{\text{red}} \end{bmatrix}, \tag{4}$$

where $\delta_w = 1$ and $\delta_\phi = \delta_\theta = \delta_\psi = 2$ are the differentiation orders of the states. The vectors $\tilde{c}_i^T$ are the i-th rows of the matrix $\tilde{C}$.

Falb (Ref. 17) suggests a decoupling control law based on feedback and feedforward terms as shown below

$$u = -K_{\text{dec}} \cdot x_F + M_{\text{dec}} \cdot u_{\text{dec}}, \tag{5}$$

where $u_{\text{dec}} = [d\theta, d\alpha, d\beta, d\delta]^T_{\text{dec}}$ is the decoupling control input. The state couplings due to the control inputs are decoupled by calculating M_{dec} as follows

$$\begin{aligned} D_D \cdot M_{\text{dec}} \cdot u_{\text{dec}} &= \operatorname{diag}(k_w, k_\phi, k_\theta, k_\psi) \cdot u_{\text{dec}} \\ \Rightarrow M_{\text{dec}} &= D_D^{-1} \cdot \operatorname{diag}(k_w, k_\phi, k_\theta, k_\psi), \end{aligned} \tag{6}$$

where k_w, k_ϕ, k_θ, and k_ψ can be freely selected.
As shown below, M_{dec} is modified within this paper to bypass pilot inputs

$$\tilde{M}_{\text{dec}} = M_{\text{dec}} + I. \tag{7}$$

where, I is the identity matirx. Note that within this work, pilot inputs are always set to zero. The feedback matrix K_{dec} is chosen as follows to decouple the states

$$K_{\text{dec}} = D_D^{-1} \cdot (C_D + \begin{bmatrix} \sum_{\mu=0}^{\delta_w - 1} q_{\mu,1} \cdot y^{\mu}_{\text{dec},1} \\ \sum_{\mu=0}^{\delta_\phi - 1} q_{\mu,2} \cdot y^{\mu}_{\text{dec},2} \\ \sum_{\mu=0}^{\delta_\theta - 1} q_{\mu,3} \cdot y^{\mu}_{\text{dec},3} \\ \sum_{\mu=0}^{\delta_\psi - 1} q_{\mu,4} \cdot y^{\mu}_{\text{dec},4} \end{bmatrix}), \tag{8}$$

where $y^{\mu}_{\text{dec},1} = \tilde{c}_i^T \cdot A^{\mu}_{\text{red}}$ corresponds to the μ-times differentiated i-th entry of the vector y_{dec}.
The parameters $q_{\mu,i}$ are selected by the applicant at their discretion. It is advisable to select the parameters $q_{\mu,i}$ and k_w, k_ϕ, k_θ, and k_ψ in a manner that ensures the system is already stable and an outer loop can be designed for tracking purposes. Choosing the parameters $q_{\mu,i}$ and $k_w, k_\phi, k_\theta, k_\psi$ according to the Table 1 ensures the stability of the system.

Table 1: Selected decoupling parameter values.

k_w	$k_\phi = k_\theta = k_\psi$	$q_{0,1}$	$q_{0,2} \ldots = q_{0,4}$	$q_{1,2} \ldots = q_{1,4}$
1	2.25	1	2.25	2.1

The decoupling approach with the parameters in Table 1 leads in the Laplace domain to the nominal helicopter model in Eq. (9).

$$\begin{aligned} G_n(s) &= \begin{bmatrix} \frac{0.752}{s+1} & \frac{0.007}{s^2+2.1\cdot s+2.25} & \frac{-0.0044}{s^2+2.1\cdot s+2.25} & \frac{0.0264}{s^2+2.1\cdot s+2.25} \\ \frac{-0.0009}{s+1} & \frac{2.477}{s^2+2.1\cdot s+2.25} & \frac{0.0198}{s^2+2.1\cdot s+2.25} & \frac{0.0462}{s^2+2.1\cdot s+2.25} \\ \frac{0.0261}{s+1} & \frac{0.0674}{s^2+2.1\cdot s+2.25} & \frac{2.176}{s^2+2.1\cdot s+2.25} & \frac{0.0197}{s^2+2.1\cdot s+2.25} \\ \frac{-0.0051}{s+1} & \frac{0.0182}{s^2+2.1\cdot s+2.25} & \frac{-0.0081}{s^2+2.1\cdot s+2.25} & \frac{2.288}{s^2+2.1\cdot s+2.25} \end{bmatrix} \\ &\approx \begin{bmatrix} \frac{0.752}{s+1} & 0 & 0 & 0 \\ 0 & \frac{2.477}{s^2+2.1\cdot s+2.25} & 0 & 0 \\ 0 & 0 & \frac{2.176}{s^2+2.1\cdot s+2.25} & 0 \\ 0 & 0 & 0 & \frac{2.288}{s^2+2.1\cdot s+2.25} \end{bmatrix} \end{aligned} \tag{9}$$

The nominal helicopter model in Eq. (9) describes the transfer behavior from u_{dec} to y_{dec}. The secondary diagonals of the nominal helicopter model in Eq. (9) are a consequence of the modified feedforward matrix. However, they are negligible due to the small numerator values. In summary, the decoupling approach of Falb (Ref. 17) provides stable first-order and second-order single-input-single output (SISO) systems. The nominal helicopter model is used for the H_∞ controller design.

MOTION SICKNESS MODEL

A motion sickness model is required to evaluate ACAH controllers for motion sickness severity and to provide the relationship between motion sickness and the sensitivity functions of the attitude angles. Therefore, the following is a brief description of how motion sickness is induced and modeled.
According to Reason (Ref. 18), motion sickness is caused by a sensory conflict within or between the visual sensors (eyes) and the motion sensors (ears) of humans. In Ref. 19, this sensory conflict is reduced to a conflict between the perceived vertical of the vestibular system (inner organ of the ear) and the expected vertical of the neural memory system (brain) based on previously experienced motion. The perceived and expected verticals represent estimates of the gravity vector. If there is a mismatch in these estimates, i.e., a conflict, the brain interprets this as a poisoning and triggers the symptoms of motion sickness until the conflict disappears.
In Refs. 6, 20, a mathematical model of vertical conflict was developed for motion in six degrees of freedom. Özkurt (Ref. 7), modified and adapted this model to fit the data on passenger sickness induced by rotorcraft motion. Hence, the reader is referred to Ref. 7 for a detailed description of the adapted model. The block diagram of this adapted model is shown in Figure 1.

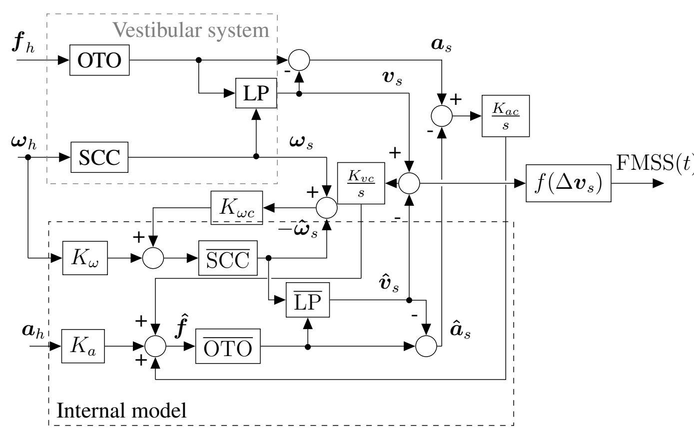

Figure 1: Block diagram of the motion sickness model from Ref. 7.

According to Figure 1, the vestibular system, consisting of the otoliths (described by the OTO transfer function) and the semicircular canals (described by the SCC transfer function), captures the gravitoinertial acceleration f_h and the angular velocity ω_h acting on the passenger's head (index h). The gravitoinertial acceleration $f_h = a_h + g_h$ and the angular velocity ω_h are necessary to resolve the sensed vertical vector

v_s within the LP block. The internal model (neural memory system) employs a similar methodology to that of the vestibular system in estimating the sensed vertical vector, denoted as $\hat{v}_s$. Consequently, the internal model contains transfer functions similar to those observed in the vestibular system. These transfer functions are indicated by a bar in Figure 1. The internal model processes the resulting specific forces on the head a_h, the angular velocities ω_h, the estimation error of the sensed angular velocities $\Delta\omega = \omega_s - \hat{\omega}_s$, the integrated vertical conflict $\int \Delta v_s \cdot dt$, and the integrated estimation error of the specific forces $\int \Delta a_s \cdot dt$ to improve the estimation of the expected vertical vector $\hat{v}_s$ during the motion exposure. The estimation errors are amplified with the gains K_{vc}, K_{ac}, and $K_{\omega c}$ and then fed back to the internal model. The whole estimation procedure of the internal model corresponds to an observer in control theory. The feedforward gains K_a and K_ω are used by the internal model to estimate the external accelerations and angular velocities. Their values are between 0 and 1 and depend on factors such as the available sight of the passenger.

If the estimated expected vertical $\hat{v}_s$ does not match to the sensed vertical v_s, the vertical conflict $\Delta v_s = v_s - \hat{v}_s$ arises. This vertical conflict is the reason for the occurrence of motion sickness symptoms. It is transformed by a nonlinear function $f(\Delta v_s)$ to calculate the fast motion sickness score (FMSS). The FMSS indicates the severity of motion sickness, which ranges from 0 to 20. It is calculated according to Eq. (10)

$$\mathrm{FMSS}(t) = \mathscr{L}^{-1}\left\{\frac{P}{\tau_1 \cdot s + 1} \cdot \mathscr{L}\left\{\frac{(||\Delta v_s(t)||/b)^2}{1 + (||\Delta v_s(t)||/b)^2}\right\}\right\}, \tag{10}$$

where $\mathscr{L}$ represents the Laplace operator.

The values of the parameters P, τ_1, and b are given in Ref. 7. According to Eq. (10), the vertical conflict vector is normalized between zero and one. Further, the normalized vertical conflict vector is accumulated by a leaky integrator and scaled with the gain P to determine the FMSS. According to Eq. (10), that the higher the squared magnitude of the vertical conflict vector $||\Delta v_s(t)||^2$, the higher the FMSS. In order to establish a connection between the motion sickness model and the rotorcraft model, it is necessary to recognize that the inputs of the motion sickness model are the outputs of the rotorcraft model. As shown below, the gravitoinertial acceleration can be calculated from the translational momentum equation of the rotorcraft in the body-fixed frame (index f).

$$\Delta\dot{v}_f + \Delta\omega_f \times v_f|_e + \Delta\omega_f \times \Delta v_f = \Delta a_f + \Delta g_f = \Delta f_f \tag{11}$$

Equation (11) considers only deviations (Δ) from the equilibrium point (index $|e$) since the used rotorcraft model is trimmed at 30 kt level flight. Consequently, the gravitoinertial acceleration can be calculated from the translational velocities, the derivation of the translational velocities, the angular velocities, and the attitude angles which are incorporated in the gravity vector Δg_f. Under the assumption of the passive motion of the passenger, the quantities of Eq. (11) are multiplied with T_{hf} to describe them in the head reference frame. The transformation matrix T_{hf} is defined in the Appendix. In Ref. 16, the motion sickness model in Figure 1 is linearized to determine the transfer behavior from the rotorcraft outputs, described in the body-fixed frame, to the vertical conflict vector Δv_s. This relationship is illustrated below

$$\Delta v_s(s) = G_{\mathrm{MS}}(s) \cdot u_{\mathrm{MS}}(s), \tag{12}$$

The transfer matrix G_{MS} is described in Ref. 16. The input vector u_{MS} contains the specific forces $a_{f,x}, a_{f,y}, a_{f,z}$, the angular velocities p, q, r, and the attitude angles ϕ, θ, ψ. The specific forces can be reconstructed from simulated rotorcraft states through Eq. (11). Within this paper, G_{MS} is necessary to provide the linkage between the sensitivity functions of the attitude angles and the vertical conflict in the sections below.

CONTROLLER DESIGN AND DESIGN OBJECTIVES

As already mentioned, the rotorcraft model is trimmed at 30 kt level flight. Therefore, an ACAH control architecture should be implemented as stated in Ref. 9. The ACAH controller has to comply with several requirements—the stability and handling qualities requirements from Refs. 9, 10 are boundary conditions for the controller. Hence, within this section the primary objectives of these requirements and their incorporation into the H_∞-control design are described. Afterwards, the parameters of the initial controller design are presented. Then, the relationship between the sensitivity functions of the attitude angles and motion sickness is derived. Finally, the systematic procedure of the controller design to reduce MS is outlined.

Stability Requirements

According to MIL-DTL-9490 (Ref. 10, p. 21), the gain margin (GM) and phase margin (PM) of the closed-loop system have to be GM ≥ 6 dB and PM ≥ 45 degrees, respectively. For SISO systems, these margins can be related to the peak value $A_{m,S}$ of the sensitivity function S as stated by Skogestad (Ref. 13, p. 34). The peak value $A_{m,S}$ is related to the GM and PM as follows

$$\mathrm{GM} = \frac{A_{m,S}}{A_{m,S} - 1}, \ \mathrm{PM} = 2 \cdot \arcsin\left(\frac{1}{2 \cdot A_{m,S}}\right). \tag{13}$$

The reformulation of Eq. (13) yields values of $A_{m,S} = 6.04$ dB and $A_{m,S} = 2.32$ dB, which satisfy the GM and PM requirements, respectively. Consequently, the PM requirement is more restrictive than the GM requirement.

Handling Quality Requirements

The Aeronautical Design Standard-33 (ADS33), as cited in Ref. 9, delineates the requisite specifications for the handling qualities of rotorcraft. These specifications are contingent upon the desired handling quality level, flight speed, and operational conditions. In the pursuit of achieving a handling quality level of 1, which is equivalent to optimal handling qualities, the aforementioned specifications become increasingly restrictive. Most of these requirements cannot be incorporated into the H_∞ control design framework and must be checked after the design.

In the revision of ADS33 (Ref. 21), the disturbance rejection bandwidth (DRB) and the disturbance rejection peak (DRP) are introduced as metrics for the disturbance rejection properties of the closed-loop system. The DRB and DRP are derived from the sensitivity functions of the variables to be tracked. The DRP is defined as the peak value of the sensitivity function and the DRB represents the frequency at which the sensitivity function crosses the -3 dB line from below. For the planned ACAH control architecture, DRB and DRP limits from Ref. 21 are summarized in Table 2.

Table 2: Specified DRB and DRP.

Axis	DRB [rad/s]	DRP [dB]
w	1	5
ϕ	0.9	5
θ	0.5	5
ψ	0.7	5

Since the DRP and DRB are related to the shape of the sensitivity function these requirements can be embedded into the H_∞ control design.

Initial H_∞ Controller Design

As stated above, the controller design is performed at the nominal design model but its robustness and performance are tested with the full helicopter model. For the controller design, the control architecture and GS/T weighting scheme in Figure 2 is considered. The exogenous signal input signal w consists of the commanded quantities r and the input disturbances u_d. The error signal z contains the weighted ouput y_w and the weighted control input u_w. The transfer behaviour from w to z is described by T_{zw} as follows

$$T_{zw}(s) = \begin{bmatrix} -W_u(s)\cdot T_u(s) & W_u(s)\cdot K(s)\cdot S(s)\cdot W_r(s) \\ W_y(s)\cdot S(s)\cdot G_n(s) & W_y(s)\cdot T(s)\cdot W_r(s) \end{bmatrix}, \tag{14}$$

where S represents the sensitivity function which describes the disturbance rejection properties of the closed-loop. T is the complementary sensitivity function that describes the tracking properties of the closed-loop. The input complementary sensitvity function $T_u(s) = K(s)\cdot G_n(s)(I+K(s)\cdot G_n(s))^{-1}$ represents the transfer behavior from u_d to $\tilde{u}$. In the case of a sufficiently decoupled system, $T_u(s)$ corresponds to $T(s)$ as shown in Ref. 22.

By defining an upper bound $\gamma = 1$ for $||T_{zw}||_\infty$, it is possible to specify the weighting transfer matrices $W_u(s), W_y(s), W_r(s)$ as approximated inverses of the specified or desired closed-loop transfer functions. This leads to the case that each entry of $T_{zw}(s)$ is smaller or equal to one. According to Eq. (14), the weighting transfer matrix $W_y(s)$ is used to shape the product $S(s)\cdot G_n(s)$ indicating that the weighting has to consider the presence of the plant model. To solve this issue, Ref. 4 proposes the following transfer matrix:

$$W_y(s) = \tilde{G}_n^{-1}(s)\cdot S_{\text{spec}}^{-1}(s), \tag{15}$$

where $\tilde{G}_n(s)$ represents a diagonal transfer matrix whose elements are designed to match the magnitudes of the nominal plant $|\tilde{G}_{n_{ii}}| \approx |G_{n_{ii}}|$. The diagonal elements of the specified sensitivity transfer matrix $S_{\text{spec}}(s)$ represent individual weighting functions for each commanded axis as shown below

$$S_{\text{spec}_{ii}}(s) = W_{S_{ii}}(s)^{-1} = \frac{s + \omega_{c,S_{ii}}\cdot A_{0,S_{ii}}}{\frac{s}{A_{m,S_{ii}}} + \omega_{c,S_{ii}}}, \tag{16}$$

where the index $i \in [w, \phi, \theta, \psi]$.

As shown in Eq. (14), the weighting transfer matrix $W_u(s)$ is used to shape the complementary sensitivity function. The matrix $W_u(s) = T_{u,\text{spec}}^{-1}$ is also diagonal and its element are specified as follows

$$W_{u,ii}(s) = \frac{s + \frac{\omega_{c,T_{ii}}}{A_{0,T_{ii}}}}{s\cdot A_{m,T_{ii}} + \omega_{c,T_{ii}}}. \tag{17}$$

The parameters $A_{m,T}$ and $A_{m,S}$ represent the high-frequency gain of the complementary sensitivity function and the sensitivity function, respectively. The parameters $A_{0,T}$ and $A_{0,S}$ are the steady state gains of the complementary sensitivity function and the sensitivity function, respectively. The parameters $\omega_{c,T}$ and $\omega_{c,S}$ are the crossover bandwidths of the complementary sensitivity function and the sensitivity function, respectively. Guidelines for the selection of these parameters are given in Refs. 4, 13, 14. For the initial H_∞ controller design, the following values are chosen for these parameters to meet the disturbance rejection and stability requirements.

Table 3: Chosen values for the initial design.

Index i	$A_{0,S}$ & $A_{0,T}$	$A_{m,S}$ & $A_{m,T}$	$\omega_{c,S}$ & $\omega_{c,T}$
w	-40&3.1 dB	2.1&-40 dB	0.7&4·π rad/s
ϕ	-40&3.1 dB	2.1&-40 dB	0.8&5·π rad/s
θ	-40&3.1 dB	2.1&-40 dB	0.3&5·π rad/s
ψ	-40&3.1 dB	2.1&-40 dB	0.3&5·π rad/s

As stated in Ref. 14, the weighting transfer matrix $W_r(s)$ should be chosen to be small and static to reduce the impact of the second column in Eq. (14) on the H_∞-norm. Since $W_r(s)$ shapes the product $K(s)\cdot S(s)$, it significantly influences the robust stability of the closed-loop system against unmodeled uncertainties and it limits the control effort. However, large values in $W_r(s)$ can lead to additional restrictions on the complementary sensitivity function as shown in Eq. (14). Hence, the values of $W_r(s)$ should be chosen small to avoid these restrictions. For the initial desgin, the diagonal entries of $W_r(s)$ are chosen as follows.

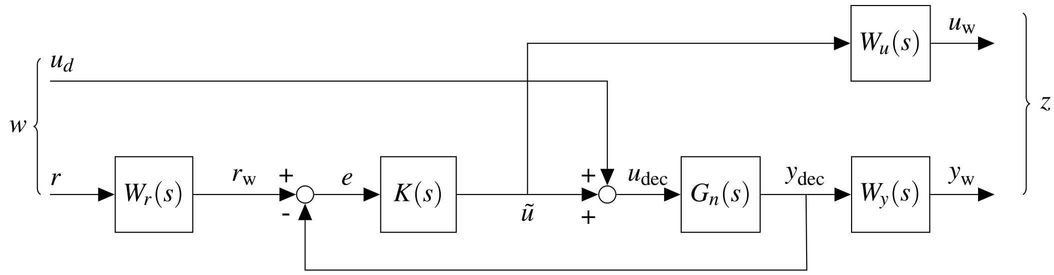

Figure 2: GS/T weighting scheme for the H_∞ controller design from Ref. 14.

Table 4: Diagonal entries of $W_r(s)$ for the initial design.

Index i	$W_{r_{ii}}(s)$ [dB]
w	-90
ϕ	-90
θ	-90
ψ	-90

The results of the initial design will be shown in the following sections.

Relation of the Vertical Conflict and Input Disturbances

For the optimization of the initial controller design regarding motion sickness, the linkage between the vertical conflict and the sensitivity functions of the attitude angles is necessary. The control architecture in Figure 3 is considered to provide the linkage. According to Figure 3, the transfer behavior from the disturbance input v_{wn} (i.e., zero mean white noise with unit intensity) to the vertical conflict vector Δv is given as

$$\Delta v_s(s) = \underbrace{\tilde{G}_{\mathrm{MS}}(s) \cdot C_{\mathrm{att}} \cdot G_n(s) \left(\tilde{V}(s) - K(s) \cdot S(s) \cdot G_n(s) \cdot \tilde{V}(s)\right)}_{H(s)} \cdot v_{wn}(s), \tag{18}$$

where $\tilde{V}(s)$ is a disturbance shaping filter such as the filters of the control equivalent turbulence input (CETI) model (Ref. 23). $\tilde{G}_{\mathrm{MS}}$ is a submatrix, associated with the attitude angles, of the motion sickness transfer matrix G_{MS} in Eq. (12). The transfer matrix $H(s)$ is further simplified by considering the sensitivity function $S_u = (I + K(s) \cdot G_n(s))^{-1}$ and complementary sensitivity function $T_u = K(s) \cdot G_n(s) \cdot S_u(s)$ at the input by relating the input to the output through the push-through rule. The push-through rule yields for the sensitivity function $S(s) \cdot G_n(s) = G_n(s) \cdot S_u(s)$. Consequently, the transfer matrix $H(s)$ can be simplified to

$$\begin{aligned} H(s) &= \tilde{G}_{\mathrm{MS}}(s) \cdot C_{\mathrm{att}} \cdot G_n(s) \left(I - K(s) \cdot G_n(s) \cdot S_u(s)\right) \cdot \tilde{V}(s), \\ &= \tilde{G}_{\mathrm{MS}}(s) \cdot C_{\mathrm{att}} \cdot G_n(s) \left(I - T_u(s)\right) \cdot \tilde{V}(s), \\ &= \tilde{G}_{\mathrm{MS}}(s) \cdot C_{\mathrm{att}} \cdot G_n(s) \cdot S_u(s) \cdot \tilde{V}(s). \end{aligned} \tag{19}$$

For decoupled systems, the input sensitivity function $S_u(s)$ is approximately equal to the sensitivity function $S(s)$. Consequently, Eq. (19) becomes

$$H(s) \approx \tilde{G}_{\mathrm{MS}}(s) \cdot C_{\mathrm{att}} \cdot G_n(s) \cdot S(s) \cdot \tilde{V}(s). \tag{20}$$

Equation (18) and Eq. (20) provide the linkage between the sensitivity function and the vertical conflict vector of the control architecture in Figure 3.
It is possible to minimize the 2-norm of the vertical conflict vector (i.e., the squared absolute value of the vertical conflict for each time step t) over the whole duration T by minimizing the root mean square (RMS) value of the vertical conflict vector since the RMS value is proportional to the 2-norm as shown below

$$\begin{aligned} ||\Delta v_s(t)||_2 &= \sqrt{\int_0^T \underbrace{||\Delta v_s(t)||^2}_{\geq 0} \cdot dt}, \\ ||\Delta v_s(t)||_{\mathrm{RMS}} &= \sqrt{\frac{1}{T}} \cdot \sqrt{\int_0^T ||\Delta v_s(t)||^2 \cdot dt}, \\ ||\Delta v_s(t)||_{\mathrm{RMS}} &= \sqrt{\frac{1}{T}} \cdot ||\Delta v_s(t)||_2. \end{aligned} \tag{21}$$

The expected RMS value of the vertical conflict represents the standard deviation of the vertical conflict for zero mean white noise input with unit intensity. Further, as stated by Skogestad (Ref. 13, p. 371), the minimization of the RMS value is equivalent to the minimization of the H_2-norm of the transfer matrix $H(s)$. Consequently, Eq. (21) becomes

$$\begin{aligned} ||\Delta v_s(t)||_{\mathrm{RMS}} &= ||H(s)||_2, \\ \sqrt{\frac{1}{T}} \cdot ||\Delta v_s(t)||_2 &= \sqrt{\sum_{kj} \frac{1}{\pi} \cdot \int_0^\infty |H_{kj}(\mathrm{j}\omega)|^2 \cdot d\omega}, \\ ||\Delta v_s(t)||_2 &= \sqrt{\sum_{kj} \frac{1}{\pi} \cdot \int_0^\infty |H_{kj}(\mathrm{j}\omega)|^2 \cdot d\omega} \cdot \sqrt{T}. \end{aligned} \tag{22}$$

According to Eq. (22), the 2-norm of the vertical conflict vector, and the squared absolute value of the vertical conflict, directly depends on the accumulated area of the squared magnitude responses of the elements in $H(\mathrm{j}\omega)$. According to Rath (Ref. 4), each element $H_{kj}(\mathrm{j}\omega)$ can be represented as follows

$$H_{kj}(s) = \sum_i R_{ki}(s) \cdot S_{ii}(s) \cdot \tilde{V}_{ij}(s), \tag{23}$$

by assuming a diagonal structure of the sensitivity function $S(s)$ and by defining the transfer matrix $R(s) = \tilde{G}_{\mathrm{MS}}(s) \cdot C \cdot G_n(s)$. The index i represents a channel of the sensitivity function. Taking into account the triangle and Cauchy-Schwarz

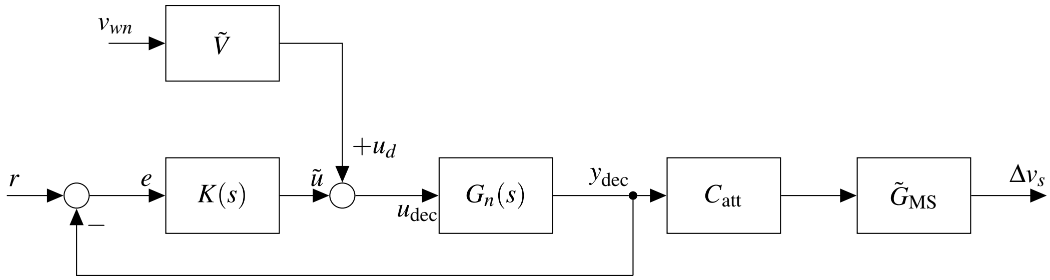

Figure 3: Considered control architecture to derive the relation between the disturbances and the vertical conflict.

inequalities, the squared magnitude of the element $H_{kj}(\mathrm{j}\omega)$ is upper bounded as follows

$$|H_{kj}(\mathrm{j}\omega)|^2 \leq 4 \cdot \sum_{i=1}^{4} \cdot |R_{ki}(\mathrm{j}\omega)|^2 \cdot |S_{ii}(\mathrm{j}\omega)|^2 \cdot |\tilde{V}_{ij}(\mathrm{j}\omega)|^2. \quad (24)$$

Inserting Eq. (24) into Eq. (22) yields the upper bound for the 2-norm of the vertical conflict vector

$$||\Delta v_s(t)||_2 \leq \sqrt{\sum_{kji} \frac{4 \cdot T}{\pi} \cdot \int_0^{\infty} |R_{ki}(\mathrm{j}\omega)|^2 \cdot |S_{ii}(\mathrm{j}\omega)|^2 \cdot |\tilde{V}_{ij}(\mathrm{j}\omega)|^2 \cdot d\omega}. \quad (25)$$

Based on Eq. (25), the 2-norm of the vertical conflict, thus the accumulated squared absolute value of the vertical conflict, can be reduced by shaping the magnitudes of sensitivity function channels within the H_∞ design.

Motion Sickness Reduction Procedure

The design procedure from Rath (Ref. 4), depicted in Figure 4, is used to reduce motion sickness systematically. As mentioned above, an initial H_∞ controller is designed to meet the stability and handling quality requirements. Based on this initial design, parameters of the sensitivity functions are selected to optimize the initial design regarding motion sickness. The adjustable parameters are the bandwidth, the peak value, and the static gain as defined in Eq. (16). These parameters shape the area below the squared magnitude response of the sensitivity function. Within this work, the focus lies only on the bandwidth. The impact of the other parameters will be investigated in future work. As shown in Figure 4, the initial design is iteratively modified to reduce the vertical conflict. The modification strategy is given through Eq. (25). The contribution of each channel of the sensitivity function to the squared 2-norm of vertical conflict is analyzed by setting an upper integration bound Ω_u. This yields

$$||\Delta v_s(t)||_2^2 \leq ||\Delta \hat{v}_s(t)||_2^2,$$
$$||\Delta \hat{v}_s(t)||_2^2 = \sum_{kji} \frac{4 \cdot T}{\pi} \cdot \int_0^{\Omega_u} |R_{ki}(\mathrm{j}\omega)|^2 \cdot |S_{ii}(\mathrm{j}\omega)|^2 \cdot |\tilde{V}_{ij}(\mathrm{j}\omega)|^2 \cdot d\omega, \quad (26)$$

where Ω_u can be chosen by the applicant. Within this work, $\Omega_u = 1$ Hz since higher frequencies do not contribute much to the vertical conflict. Based on Eq.(26), the scaling factor below is used to modify the bandwidth of the sensitivity functions systematically

$$m_i = \frac{4 \cdot T}{\pi} \cdot \frac{\sum_{kj} \int_0^{\Omega_u} |R_{ki}(\mathrm{j}\omega)|^2 \cdot |S_{ii}(\mathrm{j}\omega)|^2 \cdot |\tilde{V}_{ij}(\mathrm{j}\omega)|^2}{||\Delta \hat{v}_s(t)||_2^2}. \quad (27)$$

As stated in Ref. 4, the scaling factor m_i represents the contribution of each control channel i on the squared 2-norm of the vertical conflict. The bandwidth of each sensitivity function channel can be modified with the scaling factor m_i as follows

$$\omega_{c,S_{ii},n+1} = \omega_{c,S_{ii},n} + m_i \cdot \Delta\omega, \quad (28)$$

where $\Delta\omega$ and n represent the step size and the iteration index respectively. The updated bandwidth from Eq. (28) is inserted into Eq. (16) to modify the sensitivity function specification. The modified sensitivity function is used to define a new weighting function W_y in Eq. (15). The new weighting function W_y is used for the new controller synthesis as shown in Figure 4. The procedure is repeated until $||T_{zw}(s)||_\infty > 1$ which indicates non-compliance with the relevant design requirements. The parameters are reset to the last iteration step to ensure compliance with the requirements, providing the final H_∞ controller design.

CONTROLLER SYNTHESIS RESULTS

In this section, the designed controllers are presented. As stated above, the initial design has to comply with the stability and handling quality requirements. To avoid pole-zero cancellations the magnitude response of the nominal plant is approximated. The approximation is performed according to the guidelines in Ref. 4. The approximations are shown in Figure 10 - Figure 13. The specified values in Table 3 and Table 4 lead to the sensitivity function in Figure 5 for the roll axis. The DRB and PM requirements are illustrated as rectangles in Figure 5. As shown in Figure 5, the sensitivity function of the initial design meets the specified requirements. For low frequencies, the sensitivity function is mainly restricted by the inverse of the product $W_{y,\phi} \cdot G_{\phi,d\alpha_{\text{dec}}}$ (yellow dashed line). As depicted in Figure 5, the yellow line violates the PM requirement at high frequencies. As stated in Ref. 4, a decoupled plant is assumed within the specifications of W_y. However, the nominal model G_n is not fully diagonal. Consequently, a perfect approximation of the diagonal elements does not ensure a perfect approximation of the diagonal elements of the

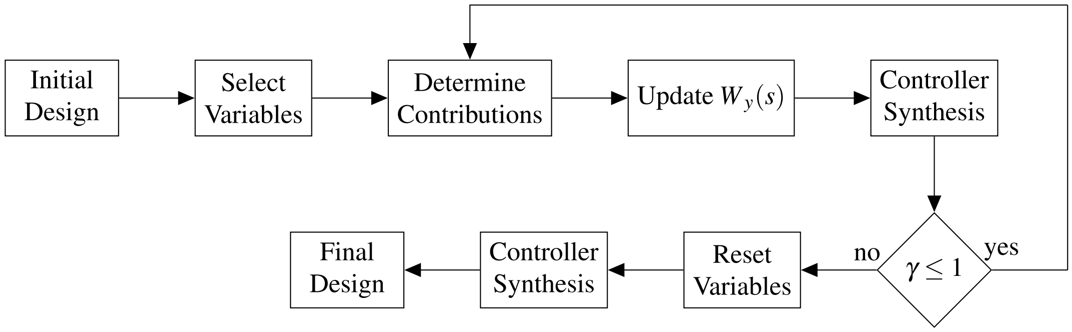

Figure 4: Systematic design procedure from Ref. 4.

inverse. Hence, the current definition of W_y can lead to violations of the PM requirement for higher frequencies. To avoid a real violation of the PM requirement by the sensitivity function, the specified sensitivity function S_{spec} mainly shapes it at high frequencies. Similar results are achieved for the other axes. Their sensitivity functions are shown in the Appendix.

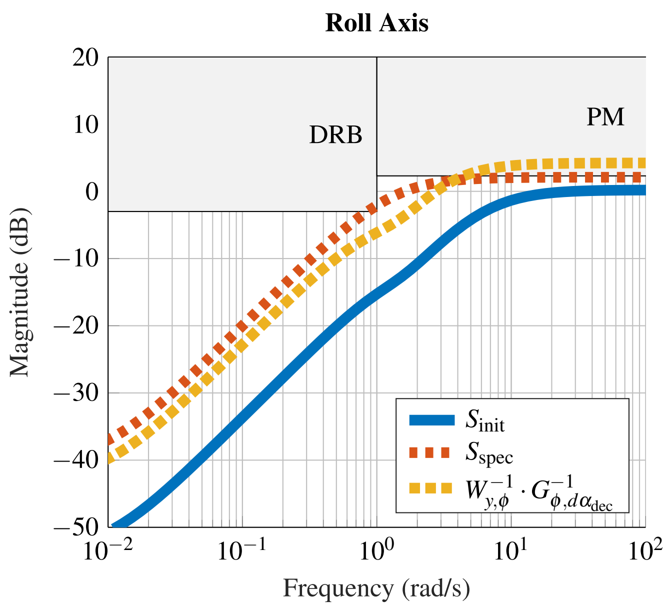

Figure 5: Sensitivity function of the initial design in roll axis.

The bandwidths of the sensitivity functions in pitch and roll axes are increased since they have the largest impact. The yaw axis is neglected due to less impact and the vertical axis is neglected since it is not in the focus of an ACAH controller. For the final design, the systematic design procedure in Figure 4 provides the sensitivity functions (green lines) below.During the systematic design procedure, the controllers are tested with the full helicopter model to check robust stability. The final design represents the last robust controller that meets the requirements. Within the roll axis, the specified sensitivity function's bandwidth ω_c is increased up to 4 rad/s while it is increased to 3 rad/s in the pitch axis. The modification of S_{spec} from Eq. (16) results in the green lines shown in Figure 6 and Figure 7.

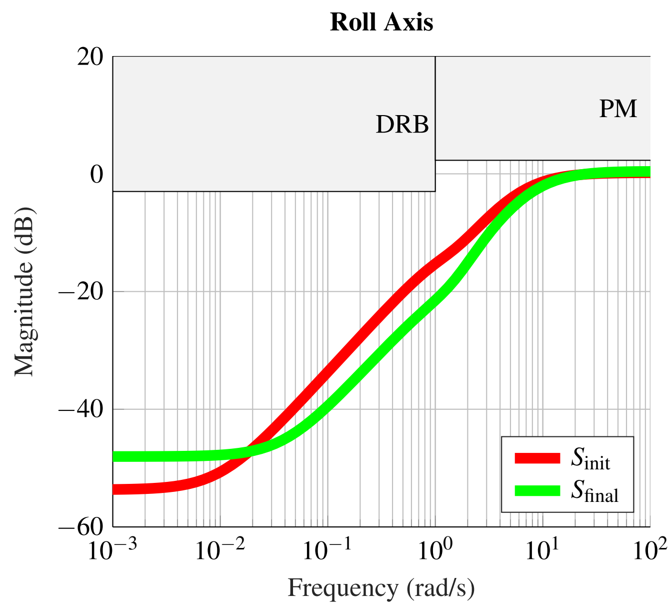

Figure 6: Sensitivity functions of the initial and final design.

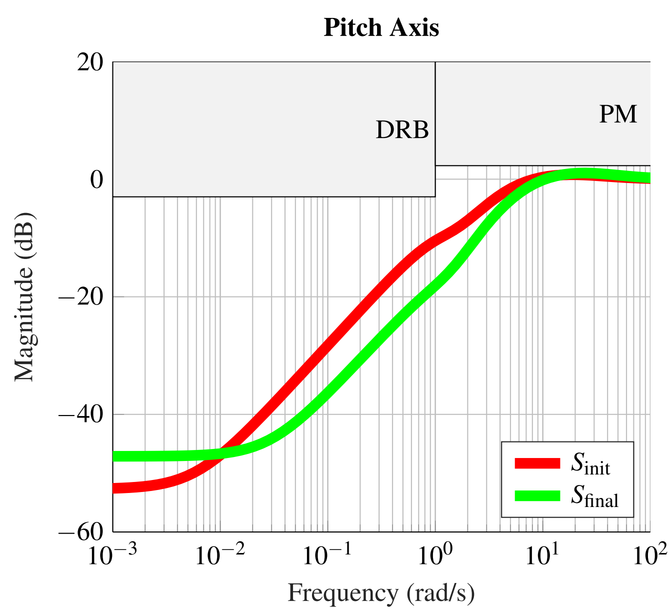

Figure 7: Sensitivity functions of the initial and final design.

The final designs in Figure 6 and Figure 7 contain higher steady state gains. Further, the final controller provides in Figure 6 and Figure 7 higher DRBs than the initial one. It also leads to lower magnitudes of the sensitivity functions between 0.02 and 12 rad/s, thus indicating a better disturbance rejection in this frequency range. Hence, it is expected that the final controller provokes less motion sickness than the initial design.

MOTION SICKNESS RESULTS

As shown in Figure 8, the gathered H_∞ controllers ($K(s)$) are applied on the original plant to analyze their performance and impact on MS during medium turbulences. Since the motion directions of typical rotorcraft are highly coupled, the control input commands provided by $\tilde{M}_{\text{dec}}\&K_{\text{dec}}$ ensure control and stabilization of the rotorcraft in each axis independently. The CETI model from Refs. 23, 24 provides control inputs from filtered white noise to simulate a gusty flight of the rotorcraft. Since the CETI model is determined for coupled rotorcraft, its output is multiplied with the inverse of $\tilde{M}_{\text{dec}}$ for a decoupled system. The output y consists of the nine rigid-body states $u, v, w, p, q, r, \phi, \theta, \psi$. Within the 'MS Model' block of Figure 8, they are transformed into the head frame. The transformed rigid-body states serve as input into the MS model from Figure 1 to assess the sickness intensity by the FMSS. Further, the matrix C_{dec} is boolean and reduces the output vector to the states that should be tracked, i.e., $y_{\text{dec}} = [w, \phi, \theta, \psi]^T$. The simulation duration is set to 20 minutes (1200 seconds) which is common for the assessment of motion sickness since sickness symptoms accumulate over time. The simulated sickness results for the initial controller and final controller are shown in Figure 9.

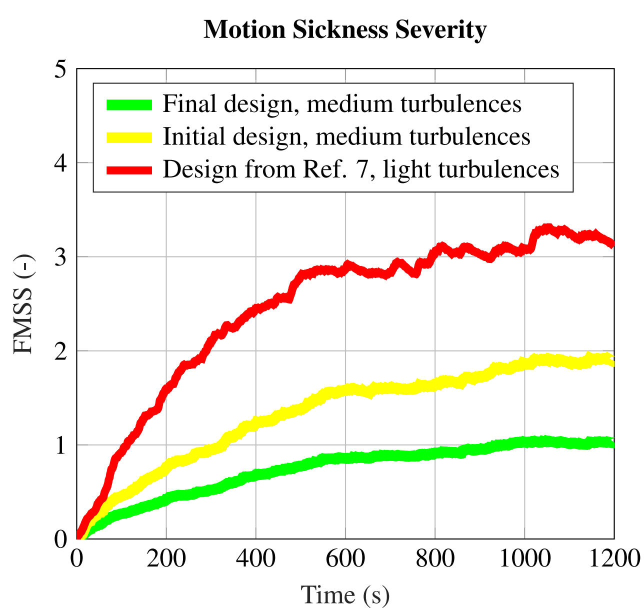

Figure 9: Simulated sickness results.

At the end of the simulation time, the initial controller leads to a FMSS=1.9. Taking into account that the FMSS ranges from 0 to 20, this sickness score is quite low. The reason for this good performance is based on the fact that the initial design already suppressed the disturbances at relevant frequencies significantly, i.e., the DRB is already high. However, the applied systematic design procedure allows to further imrpove the ride comfort through the final design. As shown in Figure 9, the final controller reduces the sickness severity over the whole exposure time. At the end of the exposure, an FMSS value of 1.03 is achieved. Consequently, the final controller reduces the sickness by 45.79% at the end of the exposure. For the same atmospheric conditions, the results in Figure 9 indicate that the final controller provides a more comfortable flight than the initial design. Compared to the classical controller design from Ref. 7, the initial and final controller, derived by the H_∞ design procedure, provides better ride comfort. The classical controller design leads to an FMSS of 3.11 during light turbulences. Despite the higher turbulence intensity, the H_∞ controllers guarantee better flight comfort than the classical controller from Ref. 7. This is the advantage of the H_∞ approach, as it allows the sensitivity function to be formed directly, whereas classic controllers have significantly fewer degrees of freedom to impose a desired shape on the sensitivity function.

CONCLUSIONS

Considering the simulation results within this paper, the following conclusions can be drawn:

1. External disturbances provoke a vertical conflict that causes sickness symptoms. As demonstrated mathematically, the severity of the sickness symptoms can be adjusted through the control system's sensitivity function.

2. The H_∞ approach is an effective method for the systematic reduction of motion sickness while maintaining compliance with stability and handling quality requirements.

3. The H_∞ approach directly shapes the sensitivity function through specifications. By increasing the bandwidth of the specified sensitivity functions, the motion sickness severity can be reduced significantly.

4. The H_∞ controllers outperform classical controllers for the shaping of the sensitivity function regarding the sickness severity and robust stability.

In summary, the controller design is the main tool to actively mitigate MS. The results confirm the need for more comprehensive tools and methods for ride quality optimization of rotorcraft that go beyond the reduction of rotor-induced vibrations.

Author contact:

S. Özkurt:	sueleyman.oezkurt@ifr.uni-stuttgart.de
S. Strobach:	st166287@stud.uni-stuttgart.de
T. Burkhardt:	tim.burkhardt@ifr.uni-stuttgart.de
W. Fichter:	fichter@ifr.uni-stuttgart.de

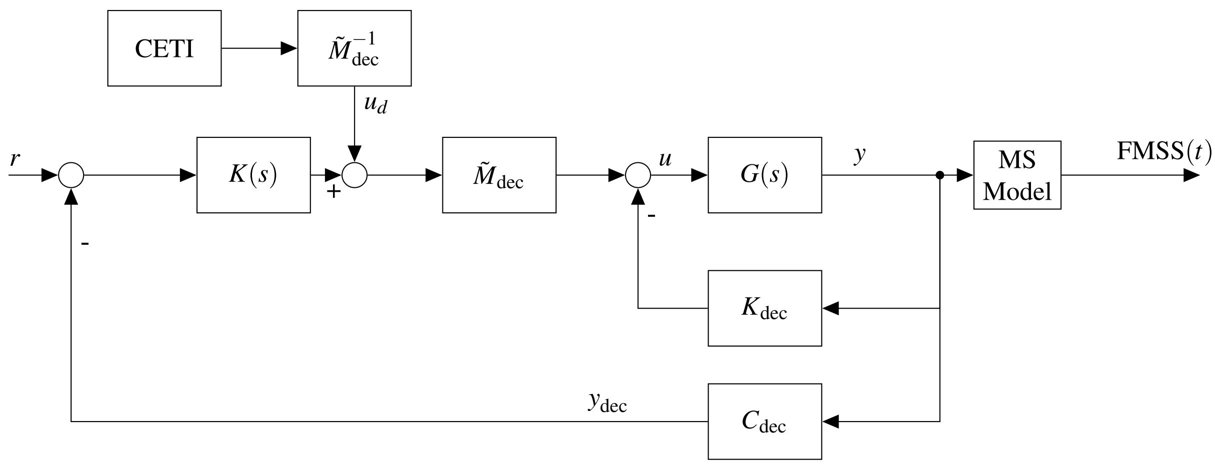

Figure 8: Simulated ACAH control architecture.

APPENDIX

Transformation from Body-Fixed to Head Frame

To describe the output of the rotorcraft in the head reference frame of the passenger, following transformation matrix is used

$$T_{hf} = \begin{bmatrix} 1 & 0 & 0 \\ 0 & -1 & 0 \\ 0 & 0 & -1 \end{bmatrix}. \tag{29}$$

Approximations of Nominal Plant's Magnitude Responses

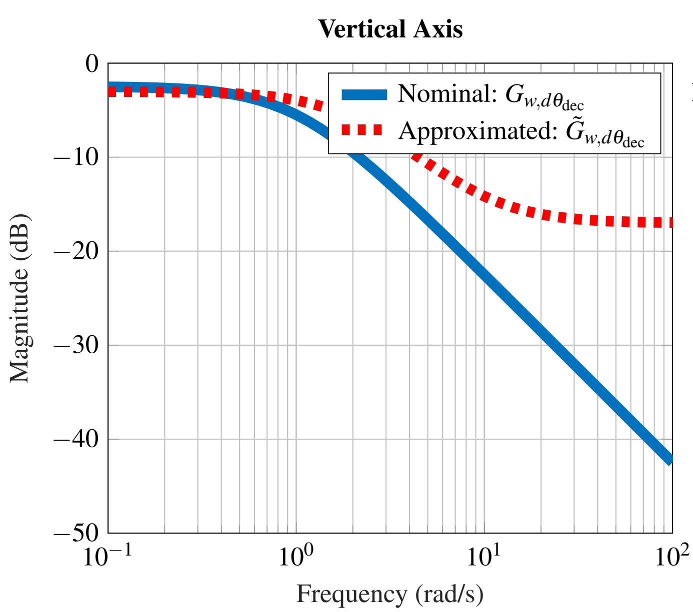

Figure 10: Transfer behaviour from collective input to vertical velocity.

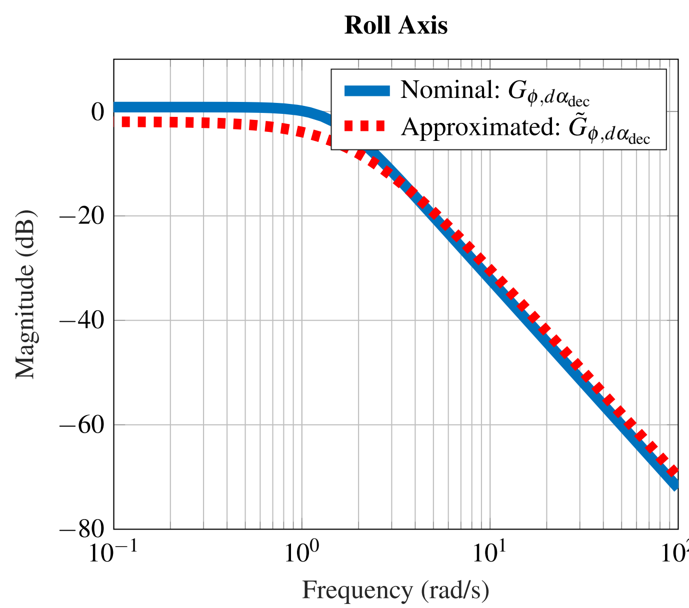

Figure 11: Transfer behaviour from lateral input to roll angle.

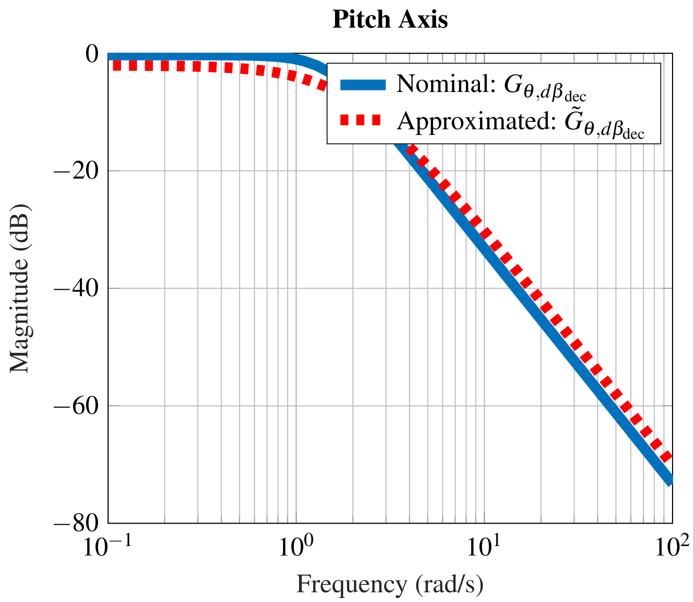

Figure 12: Transfer behaviour from longitudinal input to pitch angle.

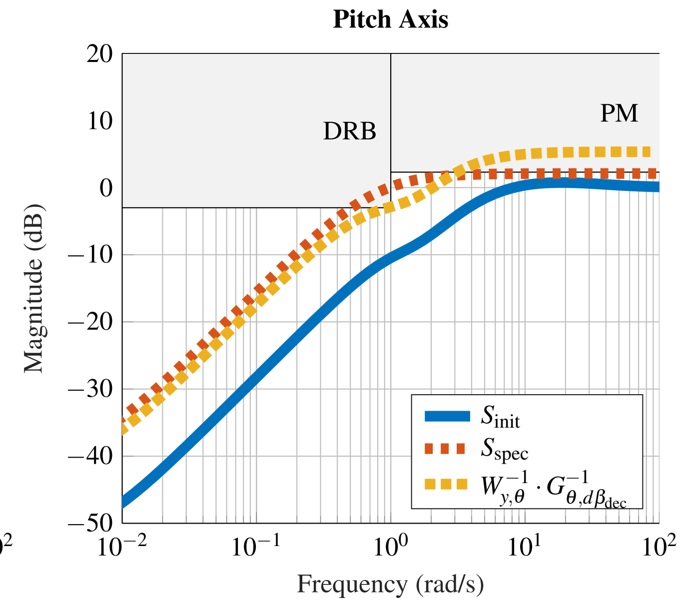

Figure 14: Sensitivity function of the initial design in pitch axis.

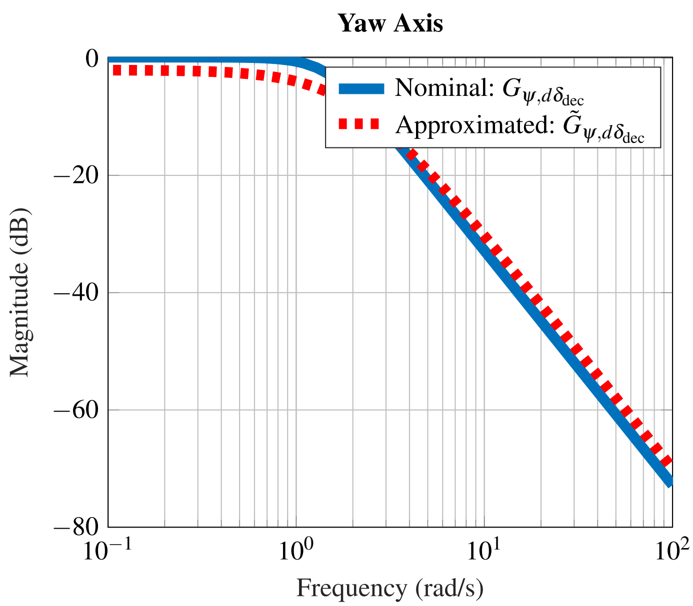

Figure 13: Transfer behaviour from pedals to yaw angle.

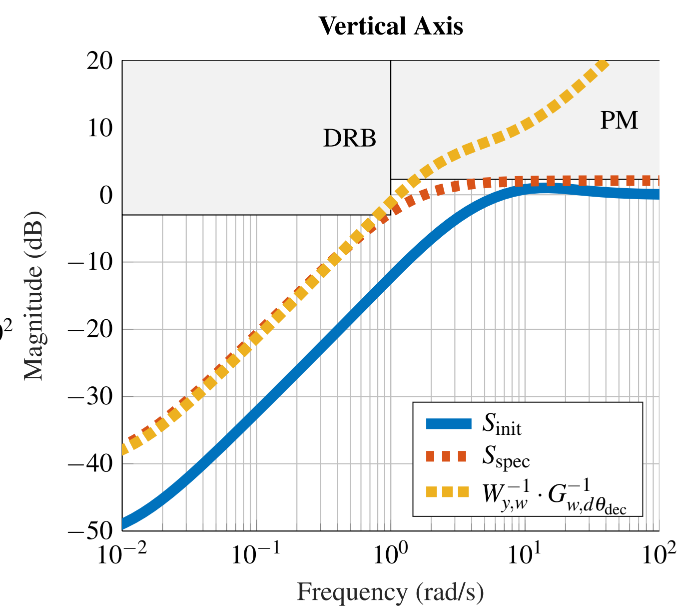

Figure 15: Sensitivity function of the initial design in vertical axis.

Sensitivity Functions The sensitivity functions of the initial design are shown below.

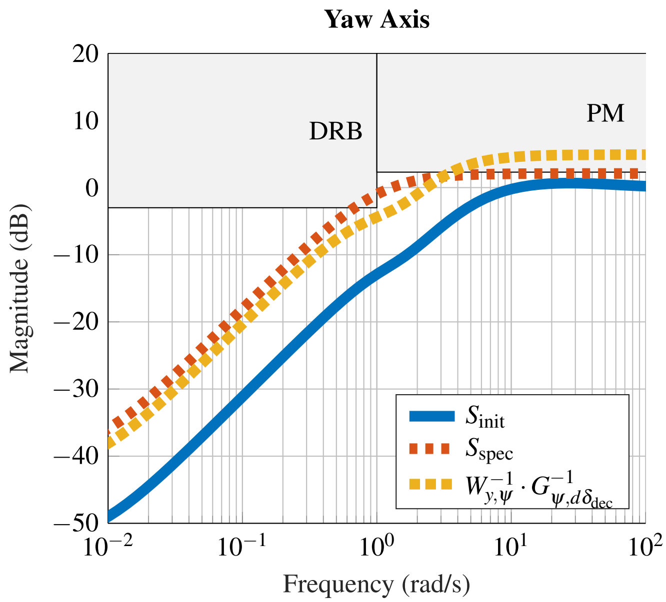

Figure 16: Sensitivity function of the initial design in yaw axis.

ACKNOWLEDGMENTS

This work is supported by the German Federal Ministry for Economic Affairs and Climate Action through the German Aviation Research Program LuFo VI-2 in the project AMI-HORATIO.

Supported by:

Federal Ministry
for Economic Affairs
and Climate Action

on the basis of a decision
by the German Bundestag

REFERENCES

1. Rabourdin, A., Maurice, J. B., Dieterich, O., and Konstanzer, P., "Blue Pulse Active Rotor Control at Airbus Helicopters - New EC145 demonstrator & flight test results," Proceedings of the 70th Annual Forum of the American Helicopter Society, May 2014.

2. Bielawa, R. L., *Rotary Wing Structural Dynamics and Aeroelasticity*, AIAA Education Series, AIAA, Virginia, 2006, pp. 251–270.

3. Hendricks, M., "The Bell 525's Smooth Ride," Proceedings of the 72nd Annual Forum of the American Helicopter Society, May 2016.

4. Rath, T., and Fichter, W., "Flight Control Design for the Systematic Improvement of Ride Qualities," *Journal of the American Helicopter Society*, Vol. 66, (2), 2021, pp. 1–14. DOI: 10.4050/JAHS.66.022003.

5. Griffin, M. J., *Handbook of Human Vibration*, Academic Press, London, England, 1990.

6. Kamiji, N., Maruo, T., Wada, T., and Doi, S., "Research on Modeling of Carsickness Based on Passenger's Motion Perception Characteristics," Proceedings of JSAE Annual Spring Congress No.59-07, 2007.

7. Özkurt, S., Burkhardt, T., Schimpf, F., and Fichter, W., "The Impact of Control Augmentation and Stability Augmentation System Parameters on Kinetosis of Rotorcraft Passengers," Proceedings of the 79th Annual Forum of the Vertical Flight Society, May 2023. DOI: 10.4050/F-0079-2023-18076.

8. Tischler, M. B., Ivler, C. M., and Mansur, M. H., "Handling-Qualities Optimization and Trade-offs in Rotorcraft Flight Control Design," Proceedings of the Royal Aeronautical Society of Rotorcraft Handling-Qualities Conference, November 2008.

9. ANON, "ADS-33E-PRF: Handling Qualities Requirements for Military Rotorcraft," , 2000.

10. ANON, "MIL-DTL-9490E: Flight Control Systems-Design, Installation and Test of Piloted Aircraft, General Specification For," , 2008.

11. Berger, T., Ivler, C. M., Berrios, M. G., Tischler, M. B., and Miller, D. G., "Disturbance Rejection Handling Qualities Criteria for Rotorcraft," Proceedings of the 72nd Annual Forum of the American Helicopter Society, May 2016.

12. Gahinet, P., and Apkarian, P., "A linear matrix inequality approach to H_∞ control," *International Journal of Robust and Nonlinear Control*, Vol. 4, (4), 1994, pp. 421–448. DOI: 10.1002/rnc.4590040403.

13. Skogestad, S., and Postlethwaite, I., *Multivariable Feedback Control*, John Wiley & Sons, 2001.

14. Christen, U., *Engineering Aspects of H_∞ Control*, Ph.D. thesis, Swiss Federal Institute of Technology Zurich, 1996.

15. Sefton, J., and Glover, K., "Pole/zero cancellations in the general H_∞ problem with reference to a two block design," *System & Control Letters*, Vol. 14, (4), 1990, pp. 295–306. DOI: 10.1016/0167-6911(90)90050-5.

16. Burkhardt, T., Özkurt, S., and Fichter, W., "Definition of Disturbance Rejection Requirements for Improved Vibrational Ride Comfort," Proceedings of the 50th European Rotorcraft Forum, September 2024.

17. Falb, P. L., and Wolowich, W. A., "Decoupling in the Design and Synthesis of Multivariable Control Systems," *IEEE Transaction on Automatic Control*, Vol. AC-12, (6), December 1967, pp. 651–659.

18. Reason, J. T., and Brand, J. J., *Motion Sickness*, Academic Press, London, 1975, pp. 102,135,210,214.

19. Bos, J., and Bles, W., "Modelling motion sickness and subjective vertical mismatch for vertical motions," *Brain Research Bulletin*, Vol. 47, (5), 1998, pp. 537 – 542.

20. Kamiji, N., Kurata, Y., Wada, T., and Doi, S., "Modeling and Validation of Carsickness Mechanism," Proceedings of International Conference and Instrumentation, Control and Information Technology, 2007. DOI: 10.1109/SICE.2007.4421156..

21. Blanken, C. L., Tischler, M. B., Lusardi, J. A., Ivler, C. M., and Lehmann, R., "Proposed Revisions to Aeronautical Design Standard – 33E (ADS-33E-PRF) Toward ADS-33F-PRF," Technical report, U.S. Army Combat CapabilitiesDevelopment Command, 2019.

22. Rath, T., *Analysis and Enhancement of Helicopter Ride Qualities in Atmospheric Turbulence*, Ph.D. thesis, Universität Stuttgart, Institut für Flugmechanik und Flugregelung, 2023.

23. Seher-Weiß, S., and von Grünhagen, W., "Development of EC135 Turbulence Models via System Identification," Proceedings of the 35th European Rotorcraft Forum, September 2009.

24. Seher-Weiß, S., and Jones, M., "Control Equivalent Turbulence Input Models for Rotorcraft in Hover and Forward Flight," *Journal of Guidance, Control and Dynamics*, Vol. 44, (8), August 2021, pp. 1517–1524. DOI: 10.2514/1.G005931.